Available online at www.sciencedirect.com
ScienceDirect
Journal of the European Ceramic Society 29 (2009) 1579–1586
www.elsevier.com/locate/jeurceramsoc

Effects of densification and mullitization on the evolution of the elastic properties of a clay-based material during firing

Pierre Pialy [a,b], Nicolas Tessier-Doyen [a,*], Daniel Njopwouo [b], Jean-Pierre Bonnet [a]

[a] *Groupe d'Etude des Matériaux Hétérogènes (GEMH, EA 3178), Ecole Nationale Supérieure de Céramique Industrielle, 47 à 73 Avenue Albert Thomas, 87065 Limoges Cedex, France*

[b] *Laboratoire de Physico-chimie des Matériaux Minéraux, Département de Chimie Inorganique, Faculté des Sciences, BP 812 Yaoundé, Cameroun*

Received 7 May 2008; received in revised form 9 September 2008; accepted 12 September 2008
Available online 14 November 2008

Abstract

The microstructural evolution of an illito-kaolinitic raw material has been characterized during firing at 10 °C/min up to 1200 °C. The strong evolution of porosity and amount of mullite formed from the viscous flux (from 1000 °C) has been quantified using dilatometric measurement, image analysis and X-ray diffraction. *In situ* ultrasonic echography has been used in order to determine the Young's modulus (E) evolution associated to the microstructural changes. This technique is highly sensitive to porosity elimination and mullite development even though an abundant viscous flux is present. For low amount of mullite (<24.7 vol.%), the E evolution observed can be easily related to porosity and mullite volume proportion changes by applying the Hashin & Shtrikman approach (lower bound). For higher mullite content, the strong experimental E increase observed between 25.9 and 51.2 GPa has been related to the transition from isolated rigid inclusions (mullite and quartz) in soft matrix (viscous flux) toward a percolating network.

Keywords: Platelets; Non-destructive evaluation; High temperature ultrasonic echography; Inclusions; Microstructure-final; Clay

1. Introduction

Echography techniques based on the propagation of ultrasonic waves in solids are widely used to control the quality of materials. By definition, these non-destructive methods exhibit the advantage to keep the sample free of damage under inspection. Ultrasonic measurements is also used at high temperature for investigating the behaviour of ceramic products, especially heterogeneous refractories.[1,2] For example, it is possible to follow *in situ* the variation of the Young's modulus of a material submitted to a thermal cycle with a suitable accuracy. Therefore this technique is particularly sensitive to possible changes in phase structure and material microstructure (pores, cracks or phase(s) formation).

The aim of the present work is to check the sensitivity of the ultrasonic technique to microstructural evolution (densification, mullite formation...) occurring during the firing of a complex natural clay-based raw material. The chosen clay material is a kaolinite–illite–quartz mixture extracted from the Lembo deposit in Cameroon, previously characterized.[3]

After presentation of the used raw material and of the sample preparations, the densification and mullitization of the studied material are described. The results of the ultrasonic echography investigation are presented and the deduced elastic properties are correlated to microstructural evolution by combining experimental characterization and predictive models.

2. Materials

2.1. Raw material

The study has been performed on a raw material (LB_3) extracted from the Lembo area (Cameroon). This unit belongs to the Bana plutonic and volcanic complex of the Cameroon volcanic line.[4] The petrologic features and a geological map of this complex have been established[5] and clay materials from Lembo have been assigned to a meteoric alteration origin.[6] Their chemical (Table 1) and estimated mineralogical (Table 2) com-

* Corresponding author. Tel.: +33 5 55 45 22 64; fax: +33 5 55 79 09 98.
E-mail address: nicolas.tessier-doyen@unilim.fr (N. Tessier-Doyen).

0955-2219/$ – see front matter.
doi:10.1016/j.jeurceramsoc.2008.09.020

Table 1
Chemical compositions (wt.%) of the studied material.

SiO_2	Al_2O_3	Fe_2O_3	MnO	MgO	CaO	Na_2O	K_2O	TiO_2	P_2O_5	Loss on ignition at 1000 °C
50.9	32.2	2.54	0.13	0.60	0.02	<l.d.[a]	4.25	0.45	0.10	9.00

[a] Limit of determination.

Table 2
Mineralogical composition (wt.%) of the studied material.

Kaolinite	Illite	Quartz	Anatase	Hematite
51 ± 4	34 ± 4	12 ± 1	0.45	2.5

positions, determined in a previous work, are very close to those commonly used in the ceramic industry.[3]

The specific surface area of LB_3 sample determined using the BET method (Micromeritics Desorb 2300A & Flowsorb II 2300) is 29 m^2/g.

The particle size distribution of the ground raw material used for the present study has been characterized by using laser diffraction Coulter granulometer (Fig. 1). The diameters of equivalent spherical grains corresponding to cumulative volumes of 10 (d_{10}), 50 (d_{50}) and 90% (d_{90}) of the total solid volume are, respectively, 0.7, 2.5 and 11.7 μm.

The value of the skeletal density, ρ_s, of LB_3 sample obtained, after grinding (till all the obtained powder grains pass through a ≈325US mesh sieve, 40 μm) and drying, by using an He pycnometer (Micromeritics AccuPyc 1330 V2. 0.3 N) is equal to 2.69 g/cm^3.

2.2. Sample preparation

The ground raw material has been granulated through a ≈187 US mesh sieve (80 μm) with the help of water (5 wt.%). Cylindrical pellets (diameter = 25 mm; thickness = 5 mm) were obtained by applying a 50 MPa uniaxial pressure. After drying for 24 h at 110 °C, 5 mm × 5 mm × 10 mm parallelepipedic samples were cut off in the previous pellets. The densification behaviour of these green parallelepipedic samples during a heating at 10 °C/min in static air was characterized in a loading dilatometer (Adamel DI 24). The load applied by the pushrod to the sample was held constant at 0.235 N. The initial porosity, $\pi_i \approx 30\%$, of the green sample has been calculated by combining the powder skeletal density (2.69 g/cm^3) and the apparent density of the dried sample (1.87 g/cm^3) determined from the dimensions and the mass of the pellet.

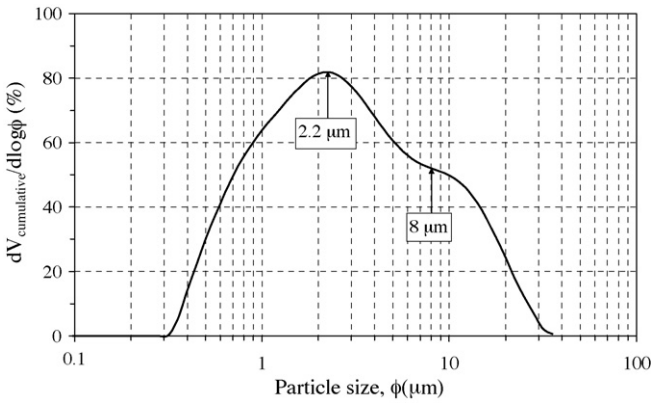

Fig. 1. Particle size distribution of the starting material.

In order to characterize the microstructural evolution of LB_3 sample during such a thermal treatment, some green pellets were heated at 10 °C/min, up to a temperature in the 1000–1200 °C range, and air quenched after a 6 min dwell.

As the "long-bar" mode ultrasonic technique requires samples with specific dimensions (≈100 × 5 × 5) mm^3 to insure reliable measurements, the previous method of preparation has been modified in order to obtain those specific samples. (120 × 50 × 6) mm^3 green samples were prepared by uniaxial pressing at 25 MPa. The cohesion of these plates was insured by adding 12 wt.% of water to dried LB_3 powder during the granulation stage. After drying at 110 °C for 24 h, pressed plates were pre-sintered at 850 °C (heating ramp = 10 °C/min) in air for 12 min and naturally cooled in a furnace. Then, bars were cut off in the fired plates.

3. Characterization methods

3.1. Microstructure of fired ceramic

The open porosity, π_o, and the apparent density ρ, of fired LB_3 specimens were determined by the Archimedes' method after immersion in water. In order to get representative values of open porosity (π_o), a 100 μm layer was eliminated before measurements from each parallel face of the sintered pellets by polishing.

For scanning electronic microscopy (SEM, Hitachi S-2500) observations, fractured LB_3 samples, previously heat-treated for 6 min at a temperature in the 1000–1200 °C range, were polished successively with SiC abrasive, 9, 6, 3 and 1 μm diamond pastes. Closed porosity (π_c) was determined by image analysis of secondary electron images of those polished samples. In order to observe mullite needles, some specimens were previously chemically etched at room temperature for 20 s with a 10 wt.% HF aqueous solution.

X-ray diffraction analysis was performed on non-oriented powders obtained after a grinding of fired LB_3 sample in a porcelain mortar. The grinding was extended till all the obtained powder grains pass through a ≈325US mesh sieve (40 μm). The diffraction diagrams were obtained using an INEL CPS (Curved Position Sensitive Detector) 120 device, working with $CuK_{\alpha 1}$ radiation (λ = 1.540598 Å) at 40 kV and 30 mA. The exposure time for qualitative analysis was 20 min. The internal-standard method was used for the quantitative analysis of the mullite developed in LB_3 sample on heating. International standard[7] of cristobalite was chosen as the reference because its linear attenu-

ation coefficient (80 cm^{-1}) is close to that of mullite (103 cm^{-1}). Moreover, the main peak (101) of cristobalite ($2\theta = 21.98°$) is isolated enough on the XRD diagram of LB_3 sample and not too far from the (220) and (111) mullite reflections (corresponding to $2\theta = 33.23°$ and 35.28°, respectively). All these reflections have been simulated by application of the so-called "peak by peak simulation method" (Voigt function) by using the "Peakoc" software. The exposure time for quantitative analysis was 12 h.

3.2. Evolution of apparent Young's modulus during firing

The evolution, during an heat treatment, of the apparent Young's modulus (E) of a material can be characterized *in situ* using ultrasonic pulse echo equipment.[8] This technique consists of measuring, all along the thermal cycle, the propagation velocity of an ultrasonic pulse in a bar of the studied material set in a furnace. The wave is produced by a transducer and transmitted to the sample by an alumina wave guide. The wave velocity is calculated from the time that separates two successive echoes. The evolution of the apparent Young's modulus of an heterogeneous material is sensitive to change in the strength of inter-atomic bonds (phase evolution), to formation or closure of cracks, to modification of porosity and to viscous flux or liquid development.[9] Consequently, this technique can be sensitive to the development of crystallized phase(s) within an amorphous matrix.[10] In the present work, the so-called "long-bar" mode analysis has been used. It requires a lateral dimension, d, of the sample lower than the ultrasonic wave length λ used ($d/\lambda \leq 0.2$) and a length of propagation (longitudinal dimension) higher than $8d$.[1] The signal treatment for the measurement of the propagation time, τ, has been performed by using the "Usanalys" software.[11] The relation between E and the propagation velocity V is:

$$E = \rho \cdot V^2 = \frac{4\rho \cdot L^2}{\tau^2} \quad (1)$$

where ρ is the apparent density, L the bar length, τ is the propagation time between two consecutive echoes. All these parameters can be temperature dependent.

The anisotropic shrinkage, observed during dilatometric measurements was taken into account for the calculation of ρ and L. Measurements were performed on 120 mm × 5 mm × 5 mm bars, pre-sintered at 850 °C, during treatments at 10 °C/min up to 1200 °C in air.

4. Microstructural evolution during sintering

4.1. Densification

Fig. 2 highlights the dilatometric behaviour of sample LB_3 in directions perpendicular and parallel to the pressure axis during an heat treatment at 10 °C/min up to 1200 °C.

Three shrinkage stages are observed:

- below 600 °C during the dehydroxylation of phyllosilicates;
- between 930 and 1000 °C simultaneously to the structural reorganization of the dehydroxylated amorphous phases. This phenomenon is usually associated to an increase of skeletal density without pore elimination;[12]
- above 1050 °C, where the fast shrinkage observed suggests the formation of a significant amount of viscous flux with a viscosity low enough to lead to grains creep under the pressure gradients generated by superficial tensile strengths, grains curvatures and necks.

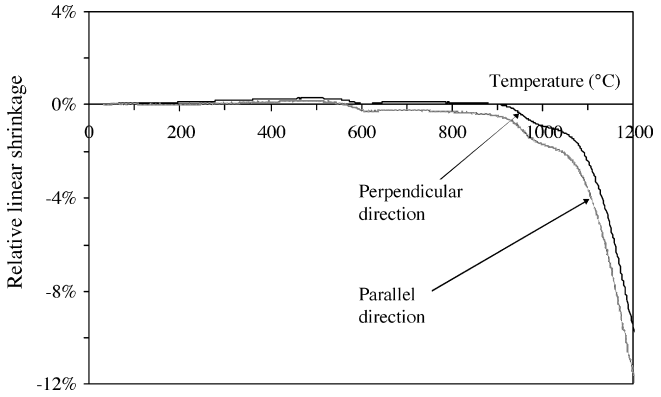

Fig. 2. Relative variation of shrinkage of the studied material by considering different directions (heating rate: 10 °C/min; static air).

The shrinkage is a little bit more important in the parallel direction. This difference, which appears during capillarity water departure ($T < 400$ °C), is enhanced by phyllosilicates dehydroxylation ($500 < T < 650$ °C) and structural reorganization ($850 < T < 1000$ °C). This behaviour is in agreement with a preferential orientation of phyllosilicate platelets corresponding to a c-axis parallel to uniaxial pressure direction.

4.2. Porosity

The influence of firing temperature on open (π_o) and closed (π_c) porosities of LB_3 samples sintered for 6 min at $1000 \leq T \leq 1200$ °C is reported in Fig. 3. The open porosity decreases from 32% at 1000 °C to nearly 0% at 1200 °C, whereas closed porosity increases from 2% until 7%. SEM images of a LB_3 sample fired at 1200 °C for 6 min are presented in Fig. 4. Very large (>15 μm) closed pores are present in this open porosity quasi free ceramic. The formation of such large closed pores

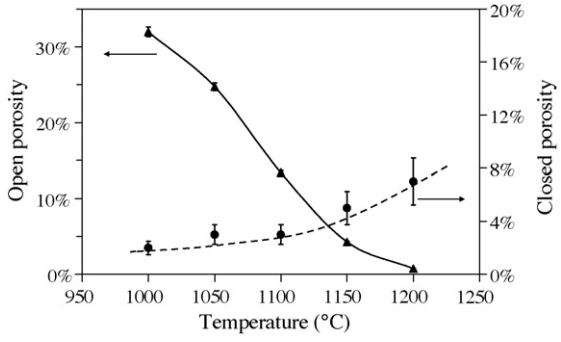

Fig. 3. Variation of open and closed porosities versus temperature of the studied material.

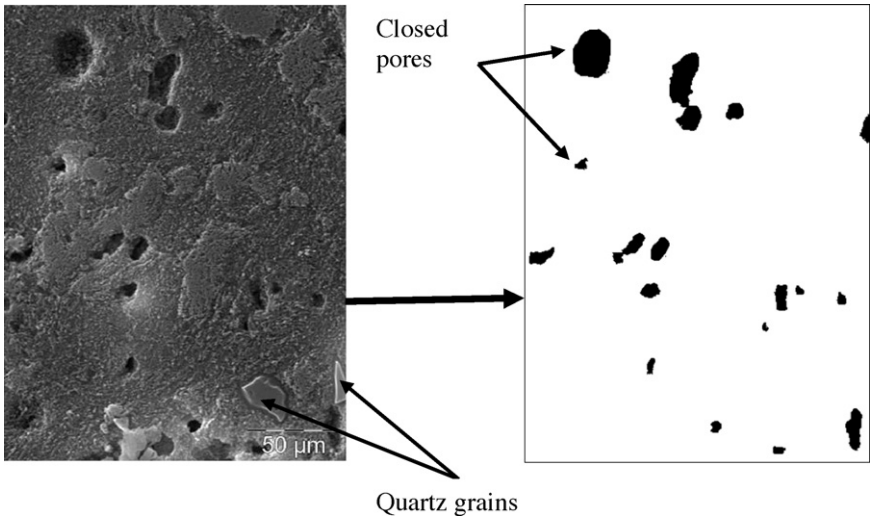

Fig. 4. SEM images of a fracture showing the size, the shape and the distribution of closed porosity of the studied material heated at 1200 °C for 6 min. Grains of quartz are also observable.

by coalescence is usually associated with a large amount of viscous flux.[13,14]

The total porosity obtained for the sample heated for 6 min at 1200 °C has been compared to the porosity deduced at 1200 °C from dilatometric analysis. The combination of the apparent density deduced from shrinkage (2.32 g/cm^3) with the skeletal density determined by helium pycnometry after grinding (2.65 g/cm^3) leads to a total porosity = 12%.

The highest porosity value deduced from dilatometric measurements at 1200 °C confirms that the load applying during experiment does not influence the observed shrinkage. It suggests also a fast densification kinetic before pores closure.

4.3. Mullitization

Concomitantly to densification, the studied material undergoes mullitization. Characteristic peaks of mullite (JCPDS file 15–0776)[15] are present on the XRD diagrams of samples heated for 6 min at $T \geq 1000$ °C (Fig. 5). The amount of mullite deduced from the quantitative analysis of samples fired for 6 min between 1000 and 1200 °C are presented in Table 3.

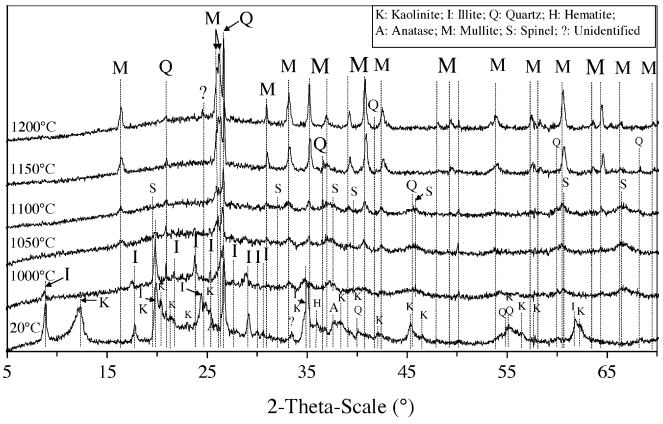

Fig. 5. XRD patterns of the studied material between ambient and 1200 °C.

Two stages of mullitization can be distinguished during heat-treatment of LB_3 sample at 10 °C/min up to 1200 °C:

- The first stage occurs below 1050 °C simultaneously to illite disappearance (Fig. 5), suggesting a possible link between both phenomena. Such a behaviour has been observed during heating of an alternate multilayer packing of kaolinite and muscovite.[16] Slaughter and Keller[17] have explained the earlier formation of mullite from illite than from kaolinite by the effect of potassium and other alkali or alkaline earth metal cations present in or near the holes of the hexagonal network of the $(SiO_4)^{4-}$ tetrahedral layers in the sheets of illite.
- The second mullitization stage corresponds to a fast increase of mullite rate (from 11 up to 30 wt.%) between 1100 and 1150 °C. The SEM image of an etched cross section (Fig. 6) shows that the mullite formed during heating up to 1200 °C is mainly made up of small needles (length < 0.5 µm) similar to those observed after formation of primary mullite from metakaolinite.[12]

It can be noticed that the spinel-like phase (JCPDS file 29–0063) present between 1000 and 1100 °C (Fig. 5) has disappeared at 1150 °C. Those results suggest the existence of a correlation between the fast mullite rate increase and the disappearance of the transitory spinel-like phase, probably formed below 1000 °C during metakaolinite structural reorganization.[12]

Table 3
Amount of mullite observed (between 1000 and 1200 °C).

T (°C)	Mullite observed (wt.%)
1000	4.7
1050	10.4
1100	11.5
1150	30.5
1200	35.6

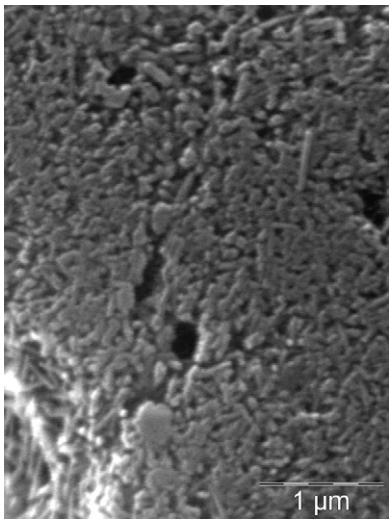

Fig. 6. SEM image of a fracture of the studied material heated at 1200 °C for 6 min (chemically etched with 10 wt.% HF for 20 s) showing the size, the shape and the distribution of mullite crystals.

5. Young's modulus evolution in relation with the microstructural changes

5.1. Experimental apparent Young's modulus of the overall material

Ultrasonic echography technique has been used in order to follow the evolution of apparent Young's modulus (E_{exp}) during densification and mullitization of LB_3 samples. Fig. 7 shows the influence of temperature on E_{exp} of the sample pre-sintered at 850 °C. The reported E_{exp} values have been calculated from experimental wave velocity and apparent density deduced from dilatometric measurements using Eq. (1).

- Below 850 °C, E_{exp} remains low and constant (about 5 GPa) in accordance with the quasi-absence of microstructural evolutions of this sample previously fired at 850 °C. It can be noticed that the α ⇄ β quartz transition near 573 °C does not lead to a significant variation of E_{exp}.

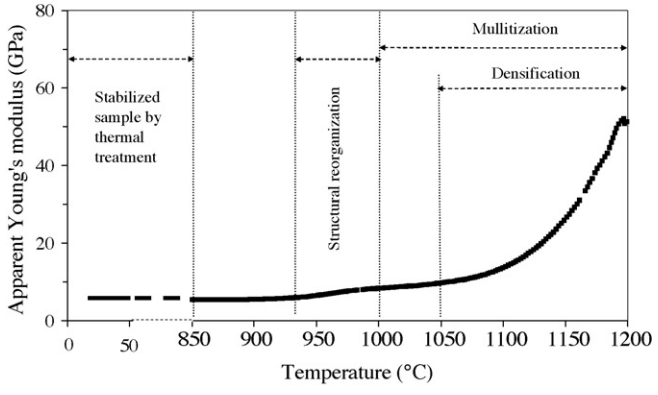

Fig. 7. Influence of temperature on the apparent Young's modulus (E_{exp}) of the sample pre-sintered at 850 °C.

- Between 930 and 1000 °C, a slight increase of apparent Young's modulus is observed concomitantly to the structural reorganization of dehydroxylated phyllosilicates.
- Above 1050 °C, E_{exp} exhibits a very strong increase from 9.7 GPa till 51.2 GPa at 1200 °C. This evolution occurs simultaneously to a decrease of the overall porosity, an increase of the amount of mullite and the development of a viscous flux with a decreasing viscosity.

5.2. Determination of the apparent Young's modulus using analytical models

5.2.1. Adapted predictive models for the description of LB_3 sample microstructure

Even if a significant amount of viscous flux must be present at least above 1100 °C, the propagation of ultrasonic waves in the studied sample shows that it is possible to calculate an equivalent Young's modulus (E^*) within the whole studied temperature range. Such configuration has already been observed for different glasses at temperature higher than glass transition temperature (T_g).[18,19]

The intrinsic modulus of each phase, their distribution in the microstructure and the porosity have obviously a great impact on the measured apparent Young's modulus of a multiphase material. The influence of phase distribution on the apparent elastic properties of LB_3 sample can be highlighted using predictive models above 1000 °C, when considering only the major phases: quartz, mullite, viscous flux and pores.

When the porosity rate is over 15%, most linear models are often inaccurate for describing the real porosity dependence.[20] The modified exponential relation proposed by Pabst et al. is used in order to take into account the porosity influence.[21] The E_0 values (skeleton Young's modulus) are then obtained using the following equation:

$$E_0 = \frac{E_{exp}}{\exp(-n \cdot \pi/1 - \pi)} \quad (2)$$

where E_{exp} is the material apparent Young's modulus, π the overall porosity volume fraction (open + closed) and n is an empirical fitting parameter equal to 2.2.[21] The corresponding E_0 values are reported in Table 4.

Depending on the quantity of mullite, different analytical models can be considered in order to describe the phases arrangement.

- For low mullite contents (typically below 1100 °C), the LB_3 sample skeleton can be described as inclusions of mullite

Table 4
LB_3 sample skeleton Young's modulus values at different temperatures.

T (°C)	E_0 (GPa)
1000	27.1
1050	22.8
1100	20.7
1150	32.2
1200	62

crystals and quartz grains in the viscous flux considered as a matrix. This configuration corresponds to the assumption of Hashin & Shtrikman (HS) for the HS lower bound, E_{HS}^- (isolated rigid inclusions in an infinite softer matrix[20]). A good agreement between the values calculated using HS model (E_{HS}^-) and the values determined from ultrasonic echography experiments has already been obtained for glass/alumina materials exhibiting an alumina volume amount ranging from 0 to 55%.[20,22]

- For higher mullite contents, the microstructure presented in Fig. 6 suggests a possible percolation between mullite needles. Therefore, the material can be described as an array of two continuous networks: a rigid one made up of mullite + quartz and a soft one corresponding to the viscous flux. This configuration does not correspond to any HS bounds microstructural hypotheses (the upper bound, E_{HS}^+, corresponding to soft inclusions in infinite rigid matrix). Such a phase arrangement can be approximately described as the combination of 2 parallel networks, the rigid one being made up of a series of linked mullite and quartz grains. This description suggests that the rigid network Young's modulus can be approximated by the Reuss relation applied to mullite and quartz grains whereas the Young's modulus of LB_3 skeleton can be determined by applying a classical rule of mixture for both rigid and viscous networks.

5.2.2. Intrinsic Young's modulus of the three condensed phases

The comparison between values deduced from experiments and analytical models requires the knowledge of intrinsic Young's modulus of the three major condensed phases (quartz, mullite and viscous flux) of LB_3 material.

The Young's modulus and Poisson's ratio of quartz (Q) and mullite (M) have been provided by literature.[23–25] The values used for calculation are reported in Table 5.

A large scattering (from about 1 to 90 GPa) is observed for the "equivalent Young's modulus" (E_{VF}^*) reported in the literature for monophase silica glasses at temperature higher than T_g.[18,19] Therefore, an attempt to estimate E_{VF}^* has been performed by assuming that the elastic behaviour of the LB_3 ceramic between 1000 and 1100 °C (when the microstructure corresponds to isolated inclusions of mullite and quartz grains in the viscous flux) can be described by applying HS^- relation first to inclusions of quartz in the "viscous flux + mullite" matrix, then to inclusions of mullite in the "viscous flux + quartz" matrix. The as-obtained values of E_{VF}^* are 15 ± 1 GPa for 1000 °C, 1050 °C and 1100 °C.

Table 5
Elastic properties of quartz and mullite at different temperatures.

T (°C)	E_Q (GPa)[20]	ν_Q[20]	E_M (GPa)[21]	ν_M[22]
20	96.6	0.075	230	0.280
1000	109.7	0.260	190	0.270
1050	110.7	0.263	188	0.270
1100	111.8	0.266	186	0.269
1150	112.8	0.269	184	0.269
1200	113.7	0.272	182	0.268

Table 6
Volume proportions of major phases respectively in the skeleton and for the overall studied material.

T (°C)	Skeleton			Overall material			
	Q (%)	M (%)	VF (%)	Total porosity (%)	Q (%)	M (%)	VF (%)
1000	13.7	4	82.3	35	8.9	2.6	53.5
1050	13.8	9	77.2	28	10	6.5	55.5
1100	13.8	10	76.2	16	11.6	8.4	64
1150	14.2	27.2	58.6	9	13	24.7	53.3
1200	14.3	32	53.7	8	13.2	29.4	49.4

It can be noticed that this result is temperature independent in the 1000–1100 °C range. For further calculation, we will consider $E_{VF}^* = 15$ GPa till 1200 °C and the Poisson's ratio of the viscous flux equal to 0.27, commonly encountered value for similar compositions.[18]

5.2.3. Results of simulation

The respective volume fractions of condensed phases were estimated from porosity rate, mass fraction and bulk density of each phase (3.21 g cm^{-3} for mullite[26], 2.65 g cm^{-3} for quartz[26] and 2.75 g cm^{-3} for flux). The flux density has been deduced from the results reported by Schilling for similar compositions.[18] The volume fractions of phase for the 5 considered temperatures are reported in Table 6.

5.2.3.1. Only the viscous flux is percolating. In order to estimate the E_0 value of a skeleton made up of isolated inclusions of quartz and mullite in a viscous flux, the following relations proposed by HS[27] for the lower bound have been applied twice.

$$E_{HS}^- = \frac{9K_{HS}^- G_{HS}^-}{3K_{HS}^- + G_{HS}^-} \quad (3)$$

K_{HS}^- and G_{HS}^- are, respectively, the bulk modulus and the shear modulus obtained from Eqs. (4) and (5)

$$G_{HS}^- = G_m + \frac{v_p}{(1/(G_p - G_m) + (6(K_m + 2G_m)v_m)/(5G_m(3K_m + 4G_m))} \quad (4)$$

$$K_{HS}^- = K_m + \frac{v_p}{(1/(K_p - K_m) + (3v_m/(3K_m + 4G_m))} \quad (5)$$

where m and p represent, respectively, the matrix and the inclusion, v_p is the volume fraction of p (G and K of each phase are respectively related to Young's modulus and Poisson's ratio by $G = E/2\,(1+\nu)$ and $K = E/3\,(1-2\nu)$).

In order to check the influence of scale level, the two following sequences of calculation have been carried out:

(i) first, application of Eq. (3) for inclusions of mullite in viscous flux, then, application of Eq. (3) for inclusions of quartz in the mullite + flux matrix;
(ii) first, application of Eq. (3) for inclusions of quartz in viscous flux, then, application of Eq. (3) for inclusions of mullite in the quartz + flux matrix.

Table 7
Young's modulus of skeleton and overall LB_3 calculated by applying twice the characteristic relation of HS lower bound considering the (i) or (ii) sequences.

T (°C)	Skeleton		Overall material	
	$E_{HS[(VF+M)+Q]^-}$ (GPa)	$E_{HS[(VF+Q)+M]^-}$ (GPa)	$E_{HS[(VF+M)+Q]^-}$ (GPa)	$E_{HS[(VF+Q)+M]^-}$ (GPa)
1000	20.5	19.9	6.3	6.1
1050	22.6	22	9.6	9.3
1100	23	22.4	15.2	14.7
1150	32.4	31.7	26	25.5
1200	35.7	35	29.5	28.9

Table 8
Skeleton and overall LB_3 material Young's modulus values calculated assuming the coexistence of two continuous networks.

T (°C)	Skeleton		Overall material
	$E_{Reuss\ (Q+M)}$ (GPa)	$E_{V[Reuss\ (Q+M)+FV}$ (GPa)	$E_{V[Reuss\ (Q+M)+FV}$ (GPa)
1000	162.6	41.1	12.6
1050	147.8	45.3	19.2
1100	145.5	46	30.3
1150	129.9	62.6	50.3
1200	128.7	67.6	55.9

The results obtained for the 5 considered temperatures for both sequences of calculation are reported in Table 7.

Values obtained by both sequences of calculation are similar (for the first sequence values are slightly higher, but the difference does not exceed 0.7 GPa for the skeleton). This shows that scale level does not have a significant influence.

5.2.3.2. Two rigid and soft percolating networks. To take into account a possible percolation of a rigid network of mullite and quartz grains, calculations have also been made considering that the connection between rigid grains corresponds to a series arrangement described by the Reuss relation[28], Eq. (6).

$$E_{Reuss(M+Q)} = \frac{1}{(v_M/E_M) + (v_Q/E_Q)} \quad (6)$$

v corresponds to the respective volume fractions of mullite and quartz in the rigid network. Then the LB_3 skeleton would correspond to the coexistence of 2 parallel percolating networks, suggesting the following relationship[29], Eq. (7).

$$E_{V[Reuss(M+Q)+VF]} = v_{(M+Q)} \cdot E_{(M+Q)} + v_{VF} \cdot E_{VF} \quad (7)$$

The corresponding skeleton and overall Young's modulus values are reported in Table 8 for different temperatures.

5.2.4. Discussion

Fig. 8 presents the evolution of experimental and overall calculated Young's modulus versus the mullite volume fraction in the overall LB_3 material.

For volume fractions of mullite lower than 24.7% ($T < 1150$ °C), experimental results are very close to the values obtained by applying twice the HS^- relations, suggesting a LB_3 microstructure made up of mullite needles and quartz grains isolated inclusions embedded by a viscous flux at high temperature.

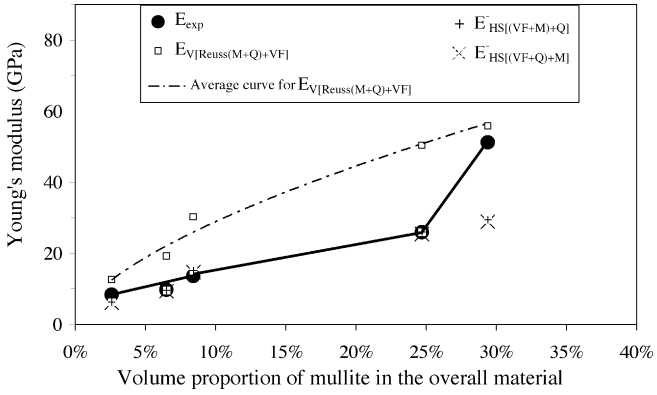

Fig. 8. High temperature apparent Young's modulus of LB3 sample versus mullite vol.%. Comparison between experimental (E_{exp}) and calculated overall values.

A very important increase of LB_3 apparent Young's modulus observed when the mullite volume ratio increases from 24.7 to 29.4% must be related to a change in phase arrangement. Nearly similar values are obtained by considering the existence of parallel rigid and soft networks. The experimental E value obtained for the highest mullite ratio ($E_{exp} = 51.2$ GPa) is almost similar to the calculated obtained value when considering the simultaneous presence of rigid and soft continuous networks ($E = 55.9$ GPa). These results suggest that the amount of mullite developed during the treatment till 1200 °C is high enough to percolate.

In this situation, the volume ratio of quartz and mullite required to obtain a continuous rigid network is very high (42.6% at 1200 °C) in comparison with the percolation threshold obtained for isotropic inclusions (≈20%[30]) then, even more, for the mullite needles.[31] This study highlights that the mullite present in the sample is only a primary-like one directly formed within the flux which keeps surrounding the mullite needles despite their important amount in the overall material.

6. Conclusion

The characterization by ultrasonic echography of a sample during sintering allows, from the apparent Young's modulus evolution, to get instantaneous information concerning mullite development on heating. In addition to its sensitivity to the amount of developed mullite, this technique is also sensitive to the evolution of connectivity between rigid grains and viscous flux present in the material at high temperature.

Acknowledgements

One of the authors, P. Pialy, is thankful to "Ecole Nationale Supérieure de Céramique Industrielle (ENSCI)" of Limoges (France) and to "Agence Universitaire de la Francophonie (A.U.F.)" for financial support.

References

1. Huger, M., Fargeot, D. and Gault, C., High-temperature measurement of ultrasonic wave velocity in refractory materials. *High Temperature-High Pressures*, 2002, **34**, 193–201.
2. Tessier-Doyen, N., Glandus, J. C. and Huger, M., Untypical Young's modulus evolution of model refractories at high temperature. *J. Eur. Ceram. Soc.*, 2006, **26**(3), 289–295.
3. Pialy, P., Nkoumbou, C., Villiéras, F., Njopwouo, D., Yvon, J., and Bonnet, J. P., Characterization for ceramic applications of clay materials from Lembo deposit, Mount Bana (Cameroon), Silicates Indust., in press.
4. Déruelle, B., Moreau, C., Nkoumbou, C., Kambou, R., Lissom, J., Njonfang, E. *et al.*, The cameroon line: a review. In *Magmatism in Extensional Structural Settings*, ed. A. B. Kampunzu and R. T. Lubala. Springer, Berlin, 1991, pp. 274–327.
5. Kuipou, G., Tchouankoue, J. P., Takahashi, N. and Sato, H., Transitional tholeiitic basalts in the Tertiary Bana volcano-plutonic complex, Cameroon Line. *J. African Earth Sci.*, 2006, **45**, 318–332.
6. Wouatong, G. A., Kitagawa, R., Takenos, Tchoua, F. M. and Njopwouo, D., Morphological transformation of kaolin minerals from granite saprolite in the Western part of Cameroon. *Clay Sci.*, 1997, **10**, 67–81.
7. Certificate of Analysis, National Institute of Standards and Technology, Standard Reference Material 1879 a, Gaithersburg, MD, 1999, pp. 1–4.
8. Suasmoro, S., Smith, D. S., Lejeune, M., Huger, M. and Gault, C., High temperature ultrasonic characterization of intrinsic and microstructural changes in ceramic $YBa_2Cu_3O_7$. *J. Mater. Res.*, 1992, **7**, 1629–1635.
9. Baudson, H., Debucquoy, F., Huger, M., Gault, C. and Rigaud, M., Ultrasonic measurement of MgO/C refractories Young's modulus at high temperature. *J. Eur. Ceram. Soc.*, 1999, **19**, 1895–1901.
10. Soro, N. S., Blanchart, P., Bonnet, J. P., Gaillard, J. M., Huger, M. and Touré, A., Sintering of kaolin in presence of ferric compound: study by ultrasonic echography. *J. de Physique IV*, 2005, **123**, 131–135.
11. Cutard, T., Fargeot, D., Gault, C. and Huger, M., Time delay and phase shift measurement of ultrasonic pulses using auto correlation methods. *J. Appl. Phys.*, 1994, **75**, 1909–1913.
12. Soro, N. S., Influence des ions fer sur les transformations thermiques de la kaolinite. Thèse doctorat n°17-2003, Université de Limoges, France, 2003, 158 pp.
13. Das, S. K. and Dana, K., Differences in densification behaviour of K- and Na-feldspar-containing porcelain bodies. *Thermochim. Acta*, 2003, **406**, 199–206.
14. Milheiro, F. A. C., Freire, M. N., Silva, A. G. P. and Holanda, J. N. F., Densification behaviour of a red firing Brazilian kaolinitic clay. *Ceram. Int.*, 2005, **31**, 757–763.
15. Powder Diffraction File Alphabetical Indexes for Experimental Patterns. Inorganic phases, sets 1–52, International Centre for Diffraction Data, Pennsylvania, 2002, 1154 pp.
16. Gridi-Bennadji, F., Matériaux de mullite à microstructure organisée composées d'assemblages muscovite–kaolinite. Thèse doctorat n°67-2007, Université de Limoges, France, 2007, 181 pp.
17. Slaughter, M. and Keller, W. D., High temperature phases from impure kaolinite. *Am. Ceram. Soc. Bull.*, 1959, **38**(12), 702–703.
18. Schilling, F. R. and Sinogeikin, S. V., Elastic properties of model basaltic melt compositions at high temperatures. *J. Geophys. Res.*, 2003, **108**(nB6), 1–13.
19. Tessier-Doyen, N., Glandus, J. C. and Huger, M., Untypical Young's modulus evolution of model refractories at high temperature. *J. Eur. Ceram. Soc.*, 2006, **26**, 289–295.
20. Tessier-Doyen, N., Étude expérimentale et numérique du comportement thermomécanique de matériaux réfractaires modèles. Thèse doctorat n°66-2003, Université de Limoges, France, 2003, 141 pp.
21. Pabst, W., Gregorová, E. and Tichá, G., Elasticity of porous ceramics—a critical study of modulus-porosity relations. *J. Eur. Ceram. Soc.*, 2006, **26**, 1085–1097.
22. Tessier-Doyen, N., Glandus, J. C. and Huger, M., Experimental and numerical study of elastic behavior of heterogeneous model materials with spherical inclusions. *J. Mater. Sci.*, 2007, **42**, 5826–5834.
23. Lakshtanov, D. L., Sinogeikin, S. V. and Bass, J. D., High-temperature phase transitions and elasticity of silica polymorphs. *Phys. Chem. Miner.*, 2007, **34**, 11–22.
24. Kumazawa, T., Ohta, S., Kanzaki, S., Sakaguchi, S. and Tabata, H., Elastic properties of mullite ceramics at elevated temperature. *J. Mater. Sci. Lett.*, 1989, **8**, 47–48.
25. Ledbetter, H., Kim, S., Balzar, D., Crudele, S. and Kriven, W., Elastic properties of mullite. *J. Am. Ceram. Soc.*, 1998, **81**(4), 1025–1028.
26. Jouenne, C. A., *Traité de céramiques et matériaux minéraux*, Septima, Paris, 657 pp.
27. Hashin, Z. and Shtrikman, S., A variational approach to the theory of the elasticity behaviour of multiphase materials. *J. Mech. Phys. Solids*, 1963, **11**, 127–140.
28. Reuss, A., Berechnung der fliessgrenze von mischkristallen auf grund der plastizitätsbedingung für einkristalle. *Zeitschrift für Angewandte Mathematik und Mechanik*, 1929, **1**, 49–58.
29. Voigt, W., *Lehrbuch der kristallphysik*. B. G. Teubner, Berlin, 1910.
30. Wu, G., Lin, J., Zhen, Q. and Zhang, M., Correlation between percolation behavior of electricity and viscoelasticity for graphite filled high density polyethylene. *Polymer*, 2006, **47**, 2442–2447.
31. Peng, G., Qiu, F., Ginzburg, V. V., Jasnow, D. and Balazs, A. C., Forming supramolecular networks from nanoscale rods in binary, phase-separating mixtures. *Science*, 2000, **288**(5472), 1802–1804.